Bone Reports 5 (2016) 70–80

Contents lists available at ScienceDirect

Bone Reports

journal homepage: www.elsevier.com/locate/bonr

Quantitative *in vivo* micro-computed tomography for assessment of age-dependent changes in murine whole-body composition

Kim L. Beaucage [a,*], Steven I. Pollmann [b], Stephen M. Sims [a], S. Jeffrey Dixon [a], David W. Holdsworth [b,c,d,**]

[a] Department of Physiology and Pharmacology, Schulich School of Medicine & Dentistry, and Bone and Joint Institute, The University of Western Ontario, London, Ontario N6A 5C1, Canada
[b] Robarts Research Institute, Schulich School of Medicine & Dentistry, and Bone and Joint Institute, The University of Western Ontario, London, Ontario N6A 5C1, Canada
[c] Department of Medical Biophysics, Schulich School of Medicine & Dentistry, and Bone and Joint Institute, The University of Western Ontario, London, Ontario N6A 5C1, Canada
[d] Department of Surgery, Schulich School of Medicine & Dentistry, and Bone and Joint Institute, The University of Western Ontario, London, Ontario N6A 5C1, Canada

ARTICLE INFO

Article history:
Received 6 February 2016
Received in revised form 20 March 2016
Accepted 4 April 2016
Available online 9 April 2016

Keywords:
Adipose tissue
Bone mineral content
Bone mineral density
Growth
Lean tissue
Skeletal tissue

ABSTRACT

Micro-computed tomography (micro-CT) is used routinely to quantify skeletal tissue mass in small animal models. Our goal was to evaluate repeated *in vivo* micro-CT imaging for monitoring whole-body composition in studies of growth and aging in mice. Male mice from 2 to 52 weeks of age were anesthetized and imaged using an eXplore Locus Ultra and/or eXplore speCZT scanner. Images were reconstructed into 3D volumes, signal-intensity thresholds were used to classify each voxel as adipose, lean or skeletal tissue, and tissue masses were calculated from known density values. Images revealed specific changes in tissue distribution with growth and aging. Quantification showed biphasic increases in total CT-derived body mass, lean and skeletal tissue masses, consisting of rapid increases to 8 weeks of age, followed by slow linear increases to 52 weeks. In contrast, bone mineral density increased rapidly to a stable plateau at ~14 weeks of age. On the other hand, adipose tissue mass increased continuously with age. A micro-CT-derived total mass was calculated for each mouse and compared with gravimetrically measured mass, which differed on average by <3%. Parameters were highly reproducible for mice of the same age, but variability increased slightly with age. There was also good agreement in parameters for the same group of mice scanned on the eXplore Locus Ultra and eXplore speCZT systems. This study provides reference values for normative comparisons; as well, it demonstrates the usefulness of *in vivo* single-energy micro-CT scans to quantify whole-body composition in high-throughput studies of growth and aging in mice.

1. Introduction

Mouse models are increasingly important in biomedical research due to their ease of genetic manipulation, ability to mimic human diseases, small body size, and relatively affordable costs (Rosenthal and Brown, 2007). When using animal models, it is important to have reference values for normative comparisons. Mouse strains often used in research today include C57BL/6, BALB/c, 129 substrains, C3H and DBA/2 mice (Crawley et al., 1997; Beck et al., 2000; Buie et al., 2008; Hankenson et al., 2008). Descriptions of the most commonly used C57BL/6 mouse include masses of wet and dry individually-isolated bones, and bone mineral density (BMD) and bone mineral content (BMC) of specific bones (*e.g.,* tibia and femur) obtained using destructive or imaging methods (Sheng et al., 1999; Brochmann et al., 2003; Somerville et al., 2004; Glatt et al., 2007). Although many parameters can be measured post-mortem, longitudinal *in vivo* studies of growing and aging mice were not possible until the advent of non-invasive imaging modalities. It is now important to establish safe, effective and reproducible approaches for assessing whole-body composition *in vivo* and to establish normal reference values for growing and aging mice.

Several *in vivo* imaging modalities exist for determining skeletal phenotypes in animals, each with differing strengths and weaknesses. Dual-energy X-ray absorptiometry (DXA) is a simple approach to determine areal BMD (aBMD) and is used for clinical diagnosis and monitoring the progression of bone diseases such as osteoporosis (Pisani et al., 2013). Determination of fat content from the scans is also possible (Pietrobelli et al., 1996; Sjogren et al., 2001; Senn et al., 2007; Halldorsdottir et al., 2009). However, DXA does not distinguish between cortical and trabecular bone, and is known to overestimate or underestimate the density of large or small bones, respectively (Judex et al., 2003). When using small animal models such as mice, the accuracy of measurement is critical; therefore, CT methods are

* Correspondence to: K. L. Beaucage, Schulich School of Medicine & Dentistry, The University of Western Ontario, London, ON N6A 5C1, Canada.
** Correspondence to: D. W. Holdsworth, Robarts Research Institute, Schulich School of Medicine & Dentistry, The University of Western Ontario, London, ON N6A 5C1, Canada.
E-mail addresses: kim.beaucage@schulich.uwo.ca (K.L. Beaucage), dholdsworth@robarts.ca (D.W. Holdsworth).

http://dx.doi.org/10.1016/j.bonr.2016.04.002

preferred. High-resolution peripheral quantitative computed tomography (HR-pQCT) is a method used clinically to determine BMD in peripheral long bones of human patients (Cheung et al., 2013) and has also been used to quantify BMD and bone microarchitecture in rodents (Beamer et al., 1996; Richman et al., 2001; Bagi et al., 2006). High-resolution magnetic resonance imaging (HR-MRI) can be used to quantify soft and hard tissues. Although radiation is not an issue in this method, high-resolution images for bone morphometry require long scan times (Donnelly, 2011). Another CT method to determine BMD is synchrotron radiation micro-CT (SRmuCT). Although SRmuCT yields images with high spatial resolution and excellent signal-to-noise ratio, it has more commonly been used for *ex vivo* rather than *in vivo* studies (Donnelly, 2011; Martin-Badosa et al., 2003; Ito et al., 2003; Ito, 2005; Raum et al., 2007). Furthermore, a limitation of this modality is that few synchrotron facilities are available (Donnelly, 2011). Therefore, the widely available technology of micro-computed tomography (micro-CT) has become a popular choice for assessment of BMD and bone microarchitecture (Kazakia et al., 2008).

Micro-CT is the gold standard for morphologic assessment and quantification of radio-opaque tissues in small samples (Donnelly, 2011; MacNeil and Boyd, 2007), including evaluation of skeletal anatomy, abnormalities and morphometry in rodent models (Hankenson et al., 2008; Ford-Hutchinson et al., 2003). Moreover, micro-CT has several advantages: it is designed specifically for imaging and analysis of small samples at high-resolution; some systems have the capacity to perform scans of whole animals such as small rodents; *in vivo* scans can be obtained rapidly without sacrificing animals; and longitudinal studies with repeated scanning of animals are possible with low radiation exposure (Glatt et al., 2007; Judex et al., 2003; Granton et al., 2010). In addition, advanced micro-CT imaging allows for accurate quantification of soft-tissue volumes. This permits assessment of whole-body composition (WBC) *in vivo*, including total body, adipose, lean and skeletal tissue parameters (Granton et al., 2010), which previously could only be evaluated post-mortem using the other imaging modalities mentioned above. Concomitant evaluation of adipose, lean and skeletal tissues will become critical in animal models as interconnected roles closely link these tissues and their functions together (Migliaccio et al., 2014; Tagliaferri et al., 2015). Although advanced *in vivo* micro-CT imaging is an emerging technique to monitor growth including normal and abnormal skeletogenesis in rodents (Guldberg et al., 2004), harnessing the power of micro-CT for WBC analyses in a rapid and comprehensive manner has been greatly overlooked. This may be attributed to the fact that advanced image analysis can be quite time consuming and tedious, as large data sets can take hundreds of hours to quantify using conventional approaches. Therefore, as micro-CT has become a preferred imaging modality for quantification of WBC in small animals, the need for high-throughput methods of analysis becomes increasingly urgent.

In the present study, we report the first use of micro-CT to monitor and repeatedly quantify WBC in groups of mice during growth and aging. WBC analysis was enabled by in-house-designed software, which quantifies whole-body parameters from scanned images, based on threshold density values of specific tissues and phantom calibrators. Although others have previously reported densities and characteristics of specific bones (Somerville et al., 2004; Glatt et al., 2007; Miller et al., 2007), there have been no previous studies using *in vivo* micro-CT to quantify changes in WBC of mice during growth and aging. In the present study, cohorts of mice were scanned at 3-week intervals from 2 to 8 weeks of age and from 8 to 26 weeks of age, with additional groups scanned at 39 and 52 weeks of age. Outcome values included: total body mass (g); adipose, lean and skeletal tissue masses (g) and mass percentages (%); bone mineral density (BMD, mg HA/cm^3); and bone mineral composition (BMC, mg HA). Femur and tibia lengths were measured using anatomical markers, and maximum BMD of femoral mid-diaphyses was quantified. Variability and internal validity of the scanning protocol were assessed. Our findings establish that non-invasive single-energy micro-CT is an accurate and effective tool for characterizing the WBC of mice during growth and aging.

2. Materials and methods

2.1. Animals

Mice, maintained on a mixed genetic background of commonly used strains (C57BL/6 × 129/Ola × DBA/2), were housed in standard cages and maintained on a 12-hour light/dark cycle, with water and standard mouse chow available *ad libitum* (2018 Teklad Global 18% protein rodent diet, Harlan Laboratories, Indianapolis, IN, USA). This study was conducted in accordance with the policies and guidelines of the Canadian Council on Animal Care and was approved by the Animal Use Subcommittee of The University of Western Ontario, London, Canada. Four cohorts of mice were studied. For cohort 1, the same mice were scanned at 2, 5 and 8 weeks of age. The mice in cohort 2 were scanned at three-week intervals from 8 to 26 weeks of age, inclusive. Cohort 3 mice were studied at 39 weeks of age. Finally, the mice in cohort 4 were scanned at 52 weeks of age (Table 1).

2.2. Micro-computed tomography (micro-CT) image acquisition

Whole-body composition of mice between 2 and 52 weeks of age was assessed using micro-CT. Mice were anesthetized with isoflurane (Forane, catalog # CA2L9100, Baxter Corporation, Mississauga, ON, Canada) and imaged using an eXplore Locus Ultra micro-CT scanner and/or an eXplore speCZT scanner (GE Healthcare Biosciences, London, ON, Canada). A calibrating phantom composed of air, water and cortical bone-mimicking epoxy having a bone mineral equivalent of 1100 mg/cm^3 (SB3; Gammex, Middleton, WI, USA) (White, 1978) was scanned together with the animals. On the eXplore Locus Ultra scanner, 1000 projection images were obtained over a single 16-second rotation (80 kVp, 55 mA tube current, 16 ms exposure). On the eXplore speCZT scanner, 900 projection images were obtained over a single 5-minute rotation (90 kVp, 40 mA tube current, 16 ms exposure). Entrance doses were 9 cGy for scans on the eXplore Locus Ultra micro-CT and 22 cGy on the eXplore speCZT, determined using a model 35614 dosimeter (Keithley Instruments, Cleveland, OH). Previous studies have shown that the $LD_{50/30}$ for mice is 5–7.6 Gy (Mole, 1957; Kohn and Kallman, 1957; Sato et al., 1981); our protocol was able to perform repeated longitudinal imaging while maintaining an acceptably low radiation dose of 9–22 cGy per scan. Moreover, other studies have shown that rodents are able to rapidly recover from individual and repeated exposures of 25–30 cGy, without affecting animal survival (Mole, 1957; Parkins et al., 1985). While still anesthetized immediately after scanning, mice were gravimetrically weighed using a portable electronic precision scale (Acculab VICON VIC-511; Sartorius Group, Germany).

Data sets were reconstructed into 3D volumes from the X-ray projection data with nominal isotropic voxel spacing of 154 μm (eXplore Locus Ultra) and 50 μm (eXplore speCZT) using a cone-beam filtered backprojection algorithm. The 50 μm volumes from the eXplore

Table 1
Mouse cohorts.

Cohort	1	2	3	4	Total
Age (weeks)	2–8	8–26	39	52	2–52
Number of mice (*n*)	8	8	8	7	31

Whole-body scans using micro-computed tomography were performed on four cohorts of male mice. In cohort 1, the same mice were scanned at three-week intervals (2, 5 and 8 weeks of age). Cohort 2 mice were scanned at three week-intervals (from 8 to 26 weeks of age). Cohort 3 was scanned only at 39 weeks and cohort 4 only at 52 weeks of age. All cohorts were scanned using the eXplore Locus Ultra system, and cohort 1 was also scanned using the eXplore speCZT system.

speCZT were then spatially-averaged to 100 μm (to improve the signal-to-noise characteristics of the volume) and 150 μm (to compare with data from the eXplore Locus Ultra). Using images of the calibrating phantom, reconstructed data were linearly rescaled into Hounsfield units (HU), with the voxel gray-level of air being −1000 HU and water 0 HU.

2.3. Analysis of whole-body composition

Using MicroView software (GE Healthcare Biosciences), three signal-intensity thresholds (−200, −30 and 190 HU) were used to classify each voxel as adipose (−200 to −31 HU), lean (−30 to 189 HU), or skeletal tissue (≥190 HU), respectively for the 154 and 150 μm scans. A different set of global thresholds was determined using MicroView for classification of adipose, lean and skeletal tissue for the 100 μm scans (−275, −40 and 250 HU, respectively). The signal-intensity thresholds were determined visually by applying thresholds to CT-derived data from several mice at each age to properly classify tissues based on anatomical locations and calibration standards, as validated previously in rodent and human data sets (Granton et al., 2010; Wyatt et al., 2015; Buie et al., 2007). In-house-designed software was used to calculate tissue masses from tissue densities of 0.95 (adipose), 1.05 (lean) and 1.92 (skeletal) g/cm^3, as listed by the International Commission on Radiation Units and Measurements (ICRU, 1989). The software computed the tissue masses first by calculating the volume of voxels (in cm^3) for each of adipose, lean, and bone tissue using the signal-intensity thresholds described above (Granton et al., 2010; Beaucage et al., 2014). Once the volume of each tissue was calculated, its contributing mass was computed as the product of the tissue volume and the corresponding tissue density. The sum of all tissue masses yielded a CT-derived estimate of whole-body mass. In addition, the software was used to calculate BMD and BMC. Briefly, BMD was computed as the ratio of the average HU value of the skeletal region of interest (ROI) to the measured HU value of the SB3 calibrator, multiplied by the known hydroxyapatite (HA)-equivalent density of the SB3 (1100 mg/cm^3). Thereafter, the program automatically computed BMC as the product of the BMD (mg HA/cm^3) and the total volume of the skeletal ROI used in the BMD calculation.

2.4. Hind-limb long-bone length

Bone lengths were determined using the line measurement tool in MicroView. Femurs were measured from the base of the lateral femoral condyle to the tip of the greater trochanter. Tibial lengths were measured from the base of the medial malleolus to the tip of the intercondylar eminence.

2.5. Determination of maximum bone mineral density

The maximum value of BMD was determined for an ROI that encompassed the mid-diaphysis of the left femur. The ROI was 33% of the total femur length along the long axis and spatially encompassed the entire mid-diaphysis in the other axes. In-house-designed software was used to determine the maximum BMD value for each femur. For consistency, when assessing these BMD values in Cohort 1 mice using 100 μm eXplore speCZT scans, we used the same threshold value as above for skeletal tissue (250 HU). Similarly, when assessing the BMD in skeletally mature mice (Cohorts 2–4) using 154 μm eXplore Locus Ultra scans, we used the same threshold value as above for skeletal tissue (190 HU). For each ROI, a histogram of BMD values was generated, plotting the gray level frequency *versus* the gray level from the indicated skeletal thresholds to the maximum value. The maximum BMD was reported as the 95th percentile of this histogram.

2.6. Statistical analyses

Data are presented as means ± standard deviation (S.D.). Differences between two groups were assessed using the Student's *t*-test. Differences among three or more groups were evaluated by two-way analysis of variance followed by a Bonferroni multiple comparisons test. Curves were fit to growth data (total body mass, lean and skeletal tissue mass, BMD and BMC) by non-linear least squares regression using two-phase association in GraphPad Prism software version 5 (GraphPad Software Inc., La Jolla, CA, USA). Curves were fit to growth data for adipose tissue mass by non-linear least squares regression using an exponential growth equation in GraphPad Prism. Differences were accepted as statistically significant at $p < 0.05$. All n values represent the number of mice used in each group.

3. Results

3.1. Imaging whole-body composition of mice during growth and aging

A total of 31 male mice, divided into four cohorts, were assessed using *in vivo* quantitative micro-CT at specific ages (Table 2). Scans obtained using the eXplore Locus Ultra micro-CT were reconstructed with nominal isotropic voxel spacing of 154 μm and rescaled into Hounsfield units. An in-house-designed program was used to assign each voxel as adipose, lean or skeletal tissue, based on threshold values. Representative mid-coronal images demonstrate the pattern of changes in whole-body composition during growth and aging (Fig. 1). At 2 weeks of age, the mice had a large amount of adipose tissue (blue) relative to their body size, which appeared to be primarily subcutaneous fat. At this age, the skeleton was still developing, as evident by the larger relative size of the appendicular skeletal elements and skull relative to overall body size, as well as incomplete mineralization of caudal vertebrae. By 5 weeks of age, we saw a marked reduction in subcutaneous adipose tissue accompanied by a corresponding increase in the proportion of lean tissue. At 52 weeks of age, mice exhibited a marked increase in visceral adiposity at the expense of lean tissue. These examples illustrate that 3D micro-CT images with appropriate thresholding can reveal the localization of tissue types within the body and changes in their distribution with growth and aging.

3.2. Quantification of whole-body composition during growth and aging

Adipose, lean and skeletal tissue volumes were converted into tissue masses by multiplying each volume by the respective tissue densities of 0.95, 1.05, and 1.92 g/cm^3 (ICRU, 1989). Time course studies revealed dramatic changes in body composition during growth, and more modest changes during aging (Fig. 2). Total CT-derived body mass showed an initial rapid increase from 2 to 8 weeks of age, followed by a slow linear increase to 52 weeks of age (Fig. 2A). Lean and skeletal tissue masses and BMC displayed a pattern similar to that of total body mass (Fig. 2C, E, F). In contrast, BMD rose rapidly until 11–14 weeks and then plateaued (Fig. 2B). Unlike other parameters, adipose tissue mass

Table 2
Percent change of whole-body composition parameters with growth and aging.

	2 weeks of age Mean ± S.D.	52 weeks of age Mean ± S.D.	Percent increase
CT-derived total body mass (g)	7.8 ± 0.2	36.3 ± 1.2	364
Adipose tissue mass (g)	1.8 ± 0.3	10.1 ± 2.6	463
Lean tissue mass (g)	4.8 ± 0.2	21.3 ± 1.2	341
Skeletal tissue mass (g)	1.2 ± 0.1	4.8 ± 0.1	306
BMD (mg HA/cm^3)	171.2 ± 6.8	339.6 ± 6.3	98
BMC (mg HA)	105.8 ± 14.5	850.9 ± 37.0	704

Data represent means ± S.D. of the indicated parameters obtained from scans on the eXplore Locus Ultra of mice at 2 weeks of age and 52 weeks of age ($n = 8$ and 7 mice, respectively). All parameters were significantly greater at 52 weeks of age compared to their values at 2 weeks of age ($p < 0.05$ determined using unpaired two-tailed Student's *t*-test).

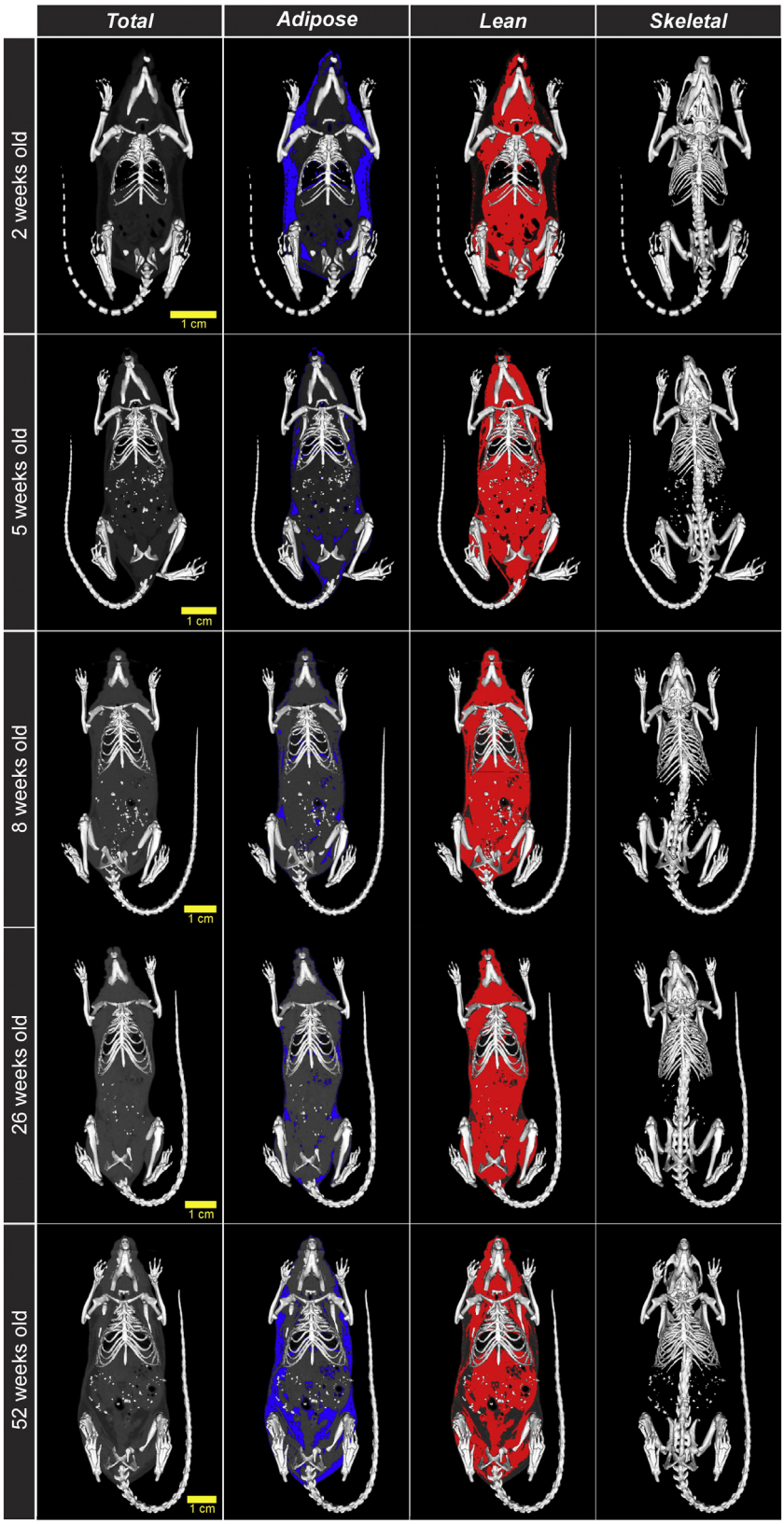

Fig. 1. Representative micro-CT images of whole-body composition showing total adipose lean and skeletal tissues. Cohorts of male mice at several ages were anesthetized for whole-body scans using the eXplore Locus Ultra micro-CT. Scans were reconstructed with nominal isotropic voxel spacing of 154 μm and rescaled into Hounsfield units using the same protocol for all ages. An in-house-designed program was used to assign each voxel as adipose lean or skeletal tissue based on threshold values. Each row shows the same mid-coronal slice from a single representative mouse at each age indicated on the left. Images were overlaid with the identified skeletal tissue (shown in white as surface-rendered images of the highest quality with no decimation). Second and third columns show adipose tissue (blue) and lean tissue (red) respectively. High-density particles in the abdomen of mice from 5 to 52 weeks of age arose from material in the animal chow. Scale bar represents 1 cm at each age point. Images are representative of at least 7 mice at each age point. (For interpretation of the references to color in this figure legend, the reader is referred to the web version of this article.)

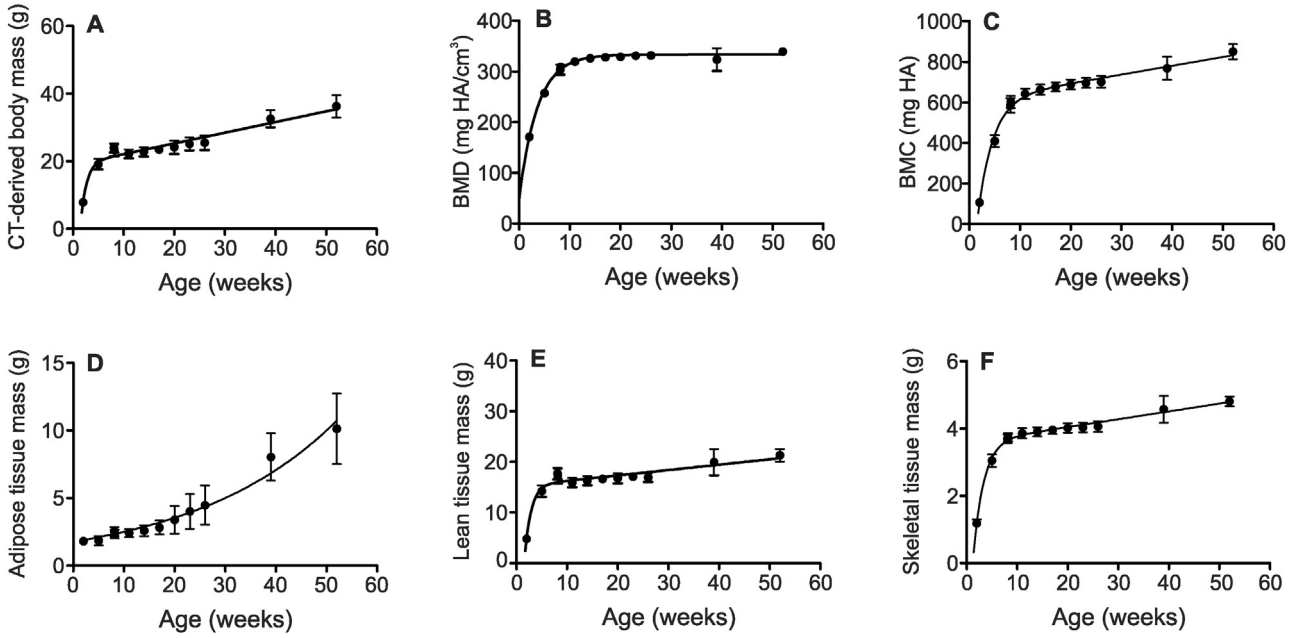

Fig. 2. Cohorts of male mice were imaged as described in the legend to Fig. 1. In-house-designed software was used to calculate tissue masses from assumed tissue densities of 0.95 (adipose), 1.05 (lean), and 1.92 (skeletal) g/cm^3, respectively. Total body mass (A) exhibited an initial rapid increase from 2 to 8 weeks of age, followed by a slow linear increase to 52 weeks. Bone mineral density (BMD, B) also showed a rapid increase until 11–14 weeks of age, but in this case was followed by a plateau. Bone mineral content (BMC, C) and lean and skeletal tissue masses (E, F) showed patterns similar to (A). In contrast, adipose tissue mass (D) displayed a distinct pattern, increasing continuously with the rate of increase rising with age. Data points for 8-week-old mice in cohorts 1 and 2 are plotted overlaid in each graph. Data are means ± S.D., $n \geq 7$ mice per age group. Curves were fit by non-linear least squares regression.

increased continuously, with the rate of increase escalating with age (Fig. 2D). The percent change in whole-body composition parameters was calculated between 2 and 52 weeks of age (Table 2). We found that lean and skeletal masses increased 300–350%, whereas adipose tissue mass showed a larger relative increase of over 460%. BMD doubled and BMC increased 7-fold, reflecting both the increase in BMD and growth in skeletal mass over time.

We next assessed the variability in whole-body composition parameters among mice at each age. Fig. 3 illustrates the range of values observed for each individual mouse. Variability was also quantified as the coefficient of variation (Table 3). Variability in CT-derived total body mass was relatively constant at each age (Fig. 3A), with coefficients of variation ranging from 7 to 9%. On the other hand, coefficients of variation for BMD and BMC were larger at 2 weeks of age decreasing to 1–2% and 4–5% in older age groups, respectively (Fig. 3B and C). Adipose tissue mass showed greatest variability (Fig. 3D), with coefficients ranging from 16% at 2 weeks of age to 26–33% in older mice. Variability of lean tissue mass was relatively constant (Fig. 3E), with coefficients ranging between 4 and 6%; whereas variability in skeletal tissue mass decreased with aging (Fig. 3F), with the coefficient of variation declining from 10% at 2 weeks to 3% at 52 weeks.

When tissue masses were expressed as a percentage of total body mass, a large decrease in adipose tissue mass was apparent from 2 to 5 weeks of age, with a corresponding increase in lean tissue mass (Fig. 3G and H). In contrast, the percentage of skeletal tissue remained relatively constant with growth and aging (Fig. 3I).

3.3. Length of long bones during growth and aging

When characterizing skeletal phenotypes of mice, the assessment of bone length has been a measurement frequently reported in the literature (Somerville et al., 2004; Glatt et al., 2007; Beamer et al., 1996; Brodt et al., 1999). Therefore, to establish external validity, we determined the lengths of hind-limb long bones using our micro-CT data sets. Using the line measurement tool in MicroView software, the right and left tibiae and femurs were measured in the scanned volume of each mouse. Tibial lengths were determined from the base of the medial malleolus to the tip of the intercondylar eminence (Fig. 4A and B). Femoral length was measured from the base of the lateral femoral condyle to the tip of the greater trochanter (Fig. 4D and E). Both bones showed rapid growth – over 2 to 8 weeks of age, tibial length increased from 10.5 to 16.3 mm and femoral length increased from 8.7 to 15.3 mm. Thereafter, there was only a slight increase in length to 17.3 mm for the tibia and 16.7 mm for the femur at 52 weeks of age. There were no significance differences between left and right bones at any age point (Fig. 4C and F).

3.4. Maximum bone mineral density

As regional variations in BMD occur within skeletal tissue, the maximum BMD value within a defined ROI better reflects the extent of compact bone mineralization. Therefore, we assessed maximum BMD of an ROI comprised of the mid-diaphyseal region of the femur. Maximum BMD values were reported as the 95th percentiles of the densities. These values displayed a rapid increase from 2 to 11 weeks of age, followed by a slow linear increase to 52 weeks of age (Fig. 5). Values for the 99th percentile showed a similar pattern as the 95th percentile, reaching 1102 ± 38 mg HA/cm^3 at 39 weeks of age, comparable to previously reported values for cortical bone BMD in mice of 1100 to 1200 mg HA/cm^3 (Windahl et al., 1999; Entezari et al., 2012). These findings reveal that maximum BMD increases during growth in mice.

3.5. Internal validity, precision and reproducibility of scanning protocols

To assess reproducibility of the scanning protocol, we examined two separate cohorts of mice at 8 weeks of age (C1 and C2). Both cohorts were scanned using the eXplore Locus Ultra micro-CT. Images were reconstructed with isotropic voxel spacing of 154 μm, rescaled into Hounsfield units and subjected to whole-body composition analysis. Similar values were obtained for the two cohorts of mice (Fig. 6). For example, the differences in gravimetric and CT-derived total body masses were only 2.9% and 2.5%, respectively. This similarity provided justification for combining data from the two cohorts of mice to obtain the time

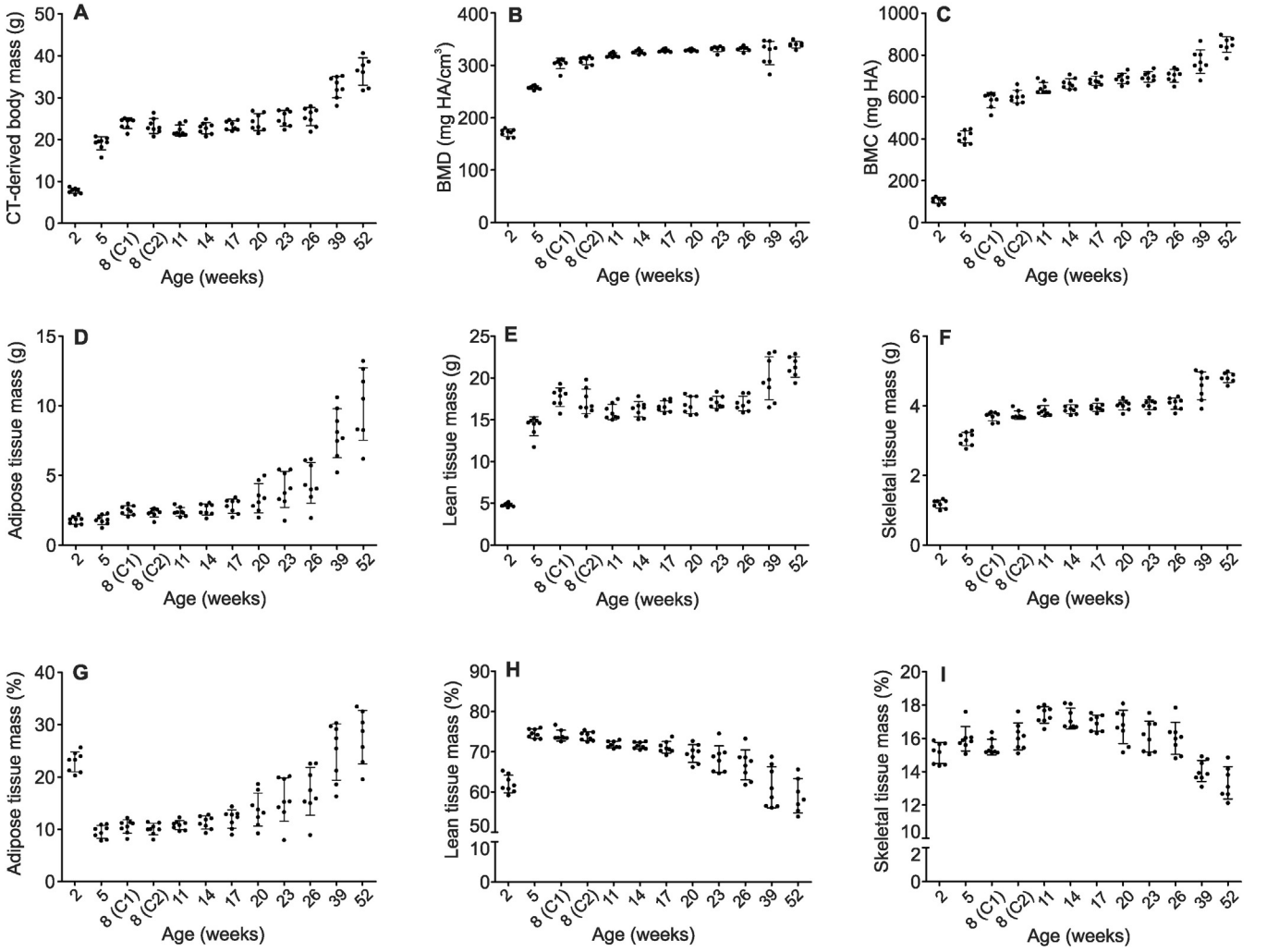

Fig. 3. Variability of whole-body composition values. Images of male mice were obtained and analyzed as described in the legends to Figs. 1 and 2. Data points (black circles) represent values of the indicated parameter for each individual mouse. Data show the vertical scatter for the age indicated numerically on the x-axis (horizontal scatter was introduced for clarity only). Eight mice were imaged at each age except 52 weeks, where $n = 7$ mice. Bars indicate mean ± S.D. for each age. Data for 8-week-old mice are presented for both cohorts 1 and 2. (A–F) illustrate parameters of whole-body composition in absolute values. (G–I) illustrate adipose, lean and skeletal tissue masses as a percentage of the total CT-derived body mass.

courses illustrated in Fig. 2. Moreover, there was no significant difference between total body masses measured gravimetrically and using micro-CT.

Next, the relationship between gravimetric and CT-derived total body mass was examined in greater detail. We compared the gravimetric to the CT-derived mass at all ages (Table 4). The computed total mass corresponded well with the weight of each mouse. The CT-derived masses were consistently less than the gravimetrically measured masses, differing by <3%. Although small, this difference was significant in mice ≥17 weeks of age. These data provide internal validation of the accuracy of our micro-CT-derived tissue mass measurements.

As described above, whole-body composition was assessed using the eXplore Locus Ultra micro-CT scanner at 154 μm resolution. However, the growing mice in cohort 1 (age 2–8 weeks) had smaller, less mineralized bones. Therefore, to confirm the accuracy of measurements made using the eXplore Locus Ultra scanner, cohort 1 was also scanned at higher resolution using the eXplore speCZT scanner. Images produced using the eXplore speCZT scanner at 50 μm isotropic voxel spacing were spatially-averaged to 100 and 150 μm. There were small, but in some cases, statistically significant differences in the CT-derived measures of total mass, BMD, BMC, and adipose, lean and skeletal tissue mass obtained using each scanner (Fig. 7). CT-derived total body mass, BMC and lean tissue mass showed the least differences among scan conditions (Fig. 7A,C, and E). Scans obtained using the eXplore Locus Ultra appeared to underestimate adipose tissue mass relative to those obtained using the eXplore speCZT scanner (Fig. 7D and G), while slightly overestimating lean tissue mass (Fig. 7E and H). Interestingly, images obtained using the eXplore speCZT scanner with 100 μm voxel spacing, appeared to underestimate BMD relative to the other conditions (Fig. 7B), while overestimating skeletal tissue mass (Fig. 7F and I).

Table 3
Coefficients of variation in whole-body composition values at selected ages.

	Coefficient of variation (%)		
	2 weeks of age	26 weeks of age	52 weeks of age
CT-derived total body mass	7.6	8.5	9.0
BMD	4.0	1.3	1.8
BMC	13.7	4.2	4.4
Adipose tissue mass	15.8	32.6	25.8
Lean tissue mass	4.3	5.2	5.8
Skeletal tissue mass	10.0	4.1	2.9

Male mice were scanned and images were analyzed as described in the legends to Figs. 1 and 2. Coefficients of variation were calculated as the ratio of the S.D. to the mean, expressed as a percentage. Eight mice were imaged at each age except 52 weeks, where $n = 7$ mice.

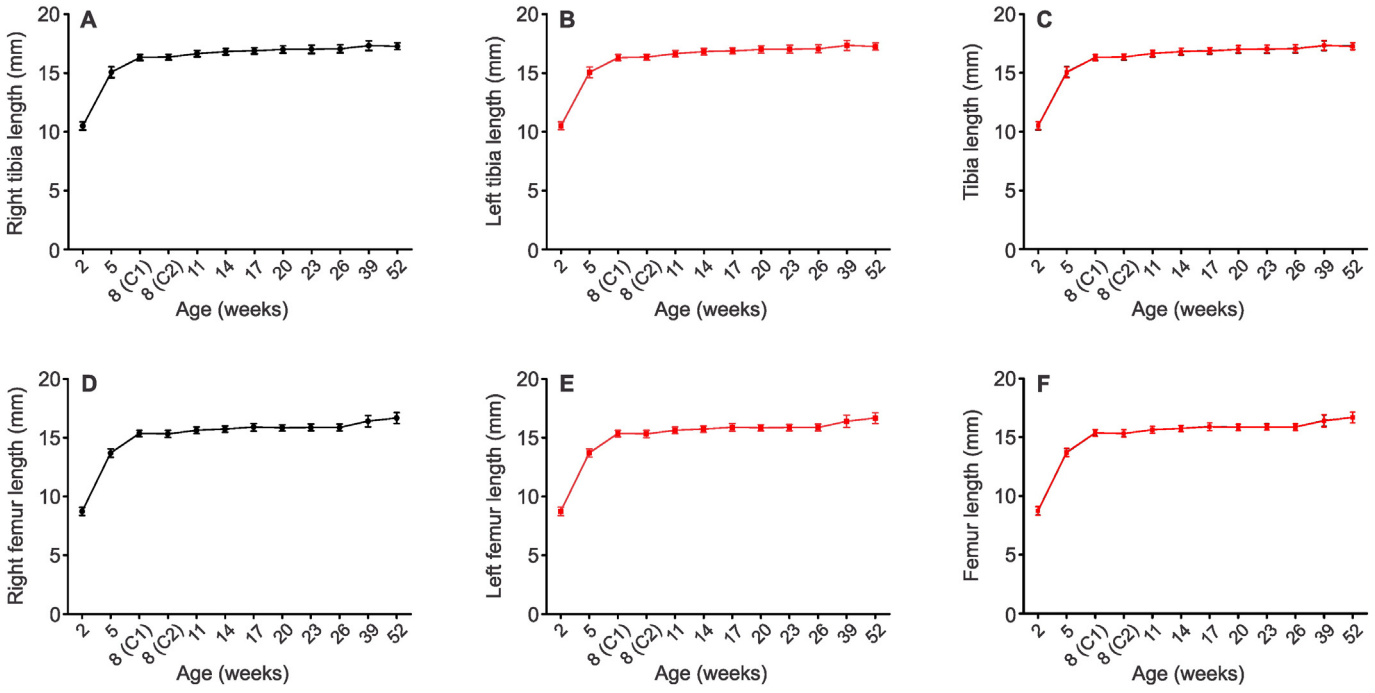

Fig. 4. Right and left tibiae and femurs were measured using the line measurement tool in MicroView from base of the medial malleolus to tip of the intercondylar eminence (for tibiae, A-B) and base of the lateral femoral condyle to tip of the greater trochanter (for femurs, D–E). Right and left tibia and femur bone lengths were overlaid respectively (C, F), revealing no significant differences between right and left limb lengths ($p > 0.05$, determined by two-way repeated measures ANOVA). Data are means ± S.D. Eight mice were imaged at each age except 52 weeks, where $n = 7$ mice.

Taken together, these data establish that non-invasive single-energy micro-CT is a valid, precise and reproducible tool for characterizing WBC of mice during growth and aging.

4. Discussion

BMD and composition are commonly reported measures of bone quantity and quality; these can be used to infer skeletal strength, fracture risk and disease state (Donnelly, 2011; Kazakia et al., 2008; Dougherty, 1996). Invasive methods have traditionally been used to determine BMD and composition, requiring post-mortem studies of whole bones in small animals. Destructive testing can be used to assess microarchitecture, mechanical tests to determine strength and elastic modulus, and ash measurements to reveal chemical composition (Donnelly, 2011; Kazakia et al., 2008). These methods are time consuming, destructive and require sacrificing the animal. Therefore, rapid, quantitative and non-invasive alternatives are desirable. Imaging modalities such as micro-CT have become a preferred avenue for measuring BMD and microarchitecture of isolated bones, in addition to assessing skeletal growth *in vivo* (Guldberg et al., 2004; Bouxsein et al., 2010).

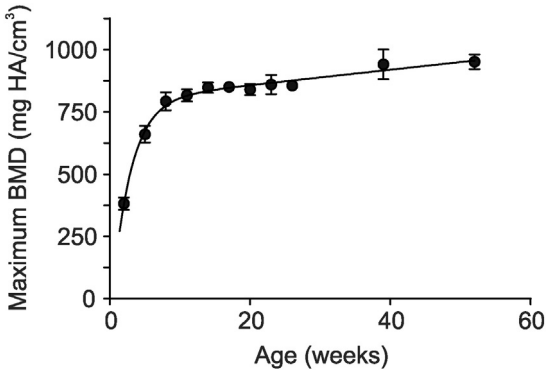

Fig. 5. Maximum bone mineral density. Mice from 2 to 8 weeks of age were scanned on the eXplore speCZT system at 50 μm and re-binned to 100 μm for these analyses. Mice from 11 to 52 weeks of age were scanned on the eXplore Locus Ultra system at 154 μm nominal voxel spacing, as described in the legends of Figs. 1 and 2. Left femurs were cropped from the whole-body images and axes were reoriented. A region of interest (ROI) that encompassed the mid-diaphysis in all three spatial directions was cropped from each of the volumes. The ROI, which included only cortical bone, was then used to determine the maximum value of BMD. Data are means ± S.D., $n = 7$ mice per age group. The curve was fit by non-linear least squares regression.

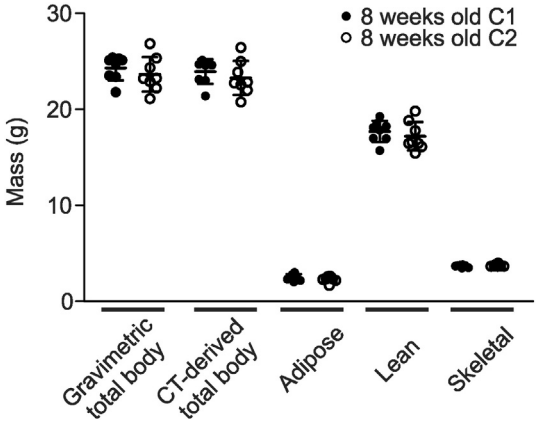

Fig. 6. Reproducibility of whole-body composition determinations. Two separate cohorts of 8-week-old male mice were imaged as described in the legend to Fig. 1 and then weighed to determine gravimetric total body mass. Data were subsequently analyzed to determine CT-derived total body mass and adipose, lean and skeletal tissue masses as described in the legend to Fig. 2. Symbols represent values of the indicated parameter for each individual mouse (filled black circles represent animals in cohort 1, and open circles represent cohort 2). Bars are means ± S.D. Eight mice were imaged in each cohort. There were no significant differences between values of gravimetric and CT-derived total body masses, providing validation of the micro-CT-derived tissue mass measurements. In addition, there were no significant differences in masses of adipose, lean or skeletal tissue between cohorts 1 and 2 ($p > 0.05$, determined by two-way ANOVA).

Table 4
Gravimetric and CT-derived total body masses of mice at each age.

Age (weeks)	Cohort	Gravimetric mass (g) Mean ± S.D.	CT-derived mass (g) Mean ± S.D.	*n*	% difference
2	1	8.0 ± 0.2	7.8 ± 0.2	8	1.9
5	1	19.5 ± 0.5	19.1 ± 0.6	8	1.7
8	1	24.3 ± 0.5	23.9 ± 0.5	8	1.6
8	2	23.6 ± 0.6	23.3 ± 0.6	8	1.6
8	1 + 2	24.0 ± 0.4	23.6 ± 0.4	16	1.6
11	2	22.7 ± 0.5	22.2* ± 0.5	8	2.2
14	2	23.1 ± 0.5	22.8 ± 0.5	8	1.5
17	2	24.0 ± 0.4	23.4* ± 0.4	8	2.3
20	2	24.8 ± 0.8	24.2* ± 0.7	8	2.4
23	2	25.8 ± 0.7	25.1* ± 0.7	8	2.8
26	2	26.2 ± 0.8	25.5* ± 0.8	8	2.9
39	3	33.2 ± 0.9	32.6* ± 0.9	8	2.1
52	4	37.2 ± 1.3	36.3* ± 1.2	7	2.5

Male mice were imaged as described in the legend to Fig. 1 and then weighed to determine gravimetric total body mass. Data were subsequently analyzed to determine CT-derived total body mass. For 8-week-old mice, data are shown for cohorts 1 and 2, individually and combined. Data are means ± S.D. *n* equals the number of mice scanned. The percent differences between means are shown in the right column. * Indicates significance difference between gravimetrically and micro-CT-derived total body masses ($p < 0.05$, assessed by two-way repeated measures ANOVA with Bonferroni's *post hoc* test).

In the present study, we investigated changes in whole-body composition with growth and aging in mice. Using non-invasive micro-CT, we were able to repeatedly scan cohorts of mice over several ages. Our results provide valuable reference data for researchers using mouse models of development, aging and disease. The whole-body masses measured using gravimetric and CT methods align well with previous reports of age-related changes in gravimetric whole-body mass of mice. Our mice more than doubled their body mass between 2 and 5 weeks of age, and exhibited ~50% increase between 4 and 8 weeks. Previous studies of growing male C57BL/6 mice reported a more modest ~30% increase between 1 and 2 months (Glatt et al., 2007), and a comparable ~47% increase in body mass (Somerville et al., 2004). Moreover, between 4 and 52 weeks of age, we observed an ~2.3-fold increase in body mass similar to previous reports of ~2.0 to 2.2-fold increase in body mass over the same period (Somerville et al., 2004; Glatt et al., 2007; Halloran et al., 2002).

To the best of our knowledge, the present study is the first to report CT-derived whole skeleton data for mice. Previous studies have reported CT-derived BMD for individual bones (vertebra, femur, tibia) (Buie et al., 2008; Beamer et al., 1996; Richman et al., 2001; Martin-Badosa et al., 2003; Amblard et al., 2003). We found that whole-body BMD values increase until 11 to 14 weeks of age, then plateau. Glatt and colleagues showed using DXA that whole-body aBMD increased rapidly up to 4 months of age in C57BL/6 mice,

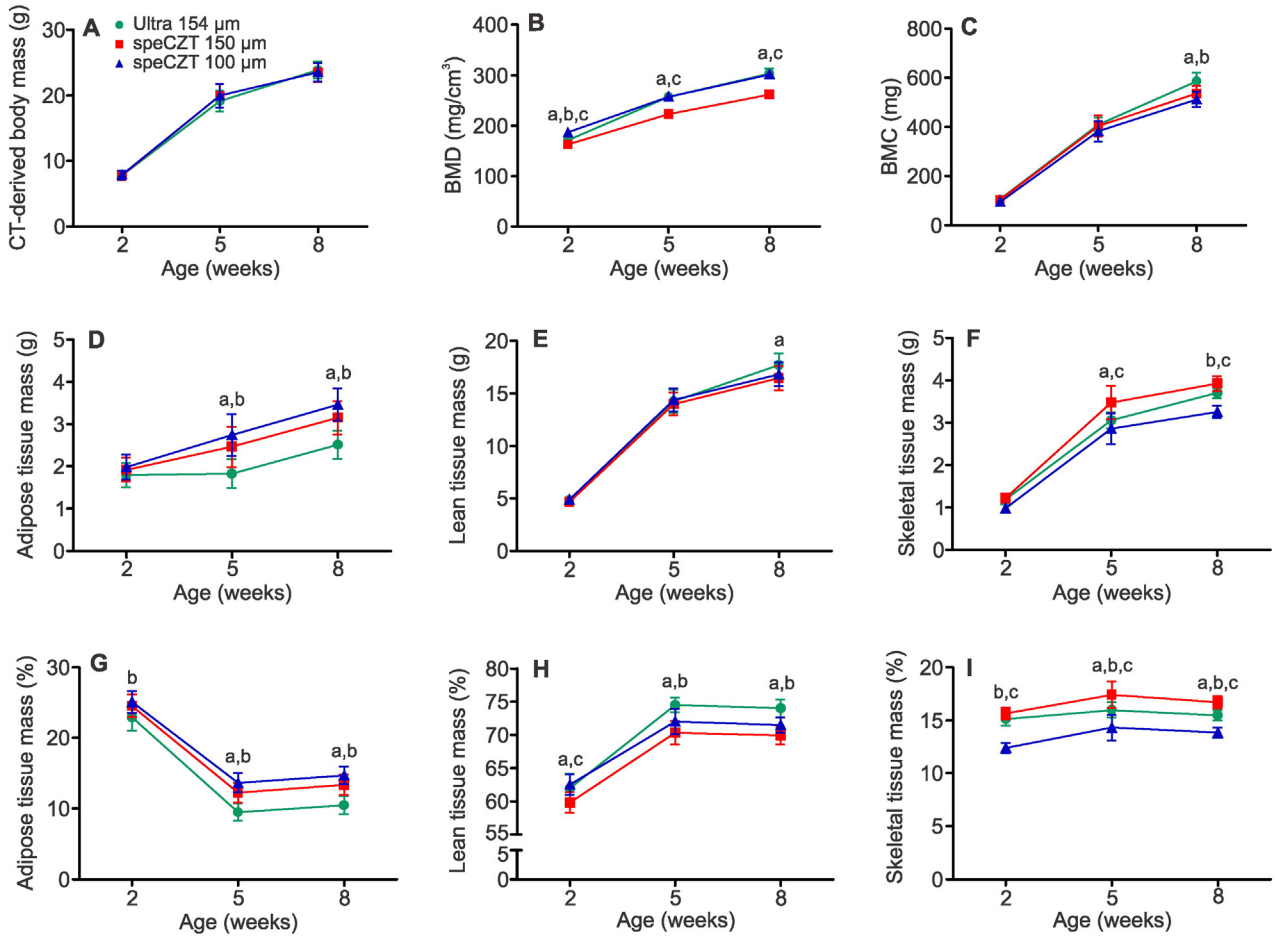

Fig. 7. Comparison of whole-body composition values determined using different scanners and voxel spacing. Cohort 1 mice were scanned at 2, 5 and 8 weeks of age on both the eXplore Locus Ultra and eXplore speCZT micro-CT scanners. Images were reconstructed to 154 µm for the eXplore Locus Ultra (green), and 150 µm and 100 µm for the eXplore speCZT (red and blue, respectively), and rescaled into Hounsfield units. Each voxel was then assigned as adipose, lean or skeletal tissue, and tissue masses were calculated. (A–F) illustrate parameters of whole-body composition in absolute values. (G–I) illustrate adipose, lean and skeletal tissue masses as a percentage of the CT-derived total body mass. Data are means ± S.D., $n = 8$ mice in each cohort. *a* indicates significant difference between the Ultra and speCZT 150 µm scans, *b* indicates significant difference between the Ultra and speCZT 100 µm scans, and *c* indicates significant difference between the speCZT 150 µm and speCZT 100 µm scans ($p < 0.05$, determined by two-way repeated measures ANOVA with Bonferroni's *post hoc* test). (For interpretation of the references to color in this figure legend, the reader is referred to the web version of this article.)

followed by a slower increase up to 12 months of age (Glatt et al., 2007). Bonkowski et al. measured aBMD and BMC in young (6–7 weeks), adult (7–10 months) and aged (28–32 months) mice. In keeping with our findings, they reported a large increase associated with growth (young-adult) and only small changes associated with aging (adult-aged) (Bonkowski et al., 2006).

Our micro-CT methodology offers the ability to quantify adipose and lean tissue components of the mouse in addition to measuring the skeletal tissues. It is known that the C57BL/6 mouse has a propensity to gain weight with age compared to other mouse models (Brochmann et al., 2003). Our data confirm other work using DXA showing a gradual increase in adipose tissue mass percent between 1 and 5 months of age, sharply increasing thereafter up to 12 months of age (Glatt et al., 2007). Interestingly, our work shows the proportion of adipose tissue at 2 weeks of age is high relative to body mass, whereas lean tissue is quite low. These values change drastically at 5 weeks of age, at which time adipose tissue mass has dropped and lean tissue mass has increased. Adiposity is important for early survival through thermal regulation by brown adipose tissue up to ~10 days of age (Xue et al., 2007). Thereafter, mice begin to develop insulation in the form of white adipose tissue until weaning at 21 days; white adipose tissue then quickly diminishes by 2 months of age (Xue et al., 2007; Kozak et al., 2010). In keeping with these previous studies, our data showed pronounced subcutaneous adiposity at 2 weeks of age followed by a drastic reduction at 5 weeks, possibly reflecting changes in the requirement for thermal insulation. Furthermore, the replacement of adipose by lean tissue may reflect increased energy demands due to ambulation and dietary changes post-weaning at 3 weeks of age.

We also found that the maximum value of BMD increases rapidly until 11 weeks of age, and is then followed by a slow linear increase. Maximum BMD values represent the degree of mineralization of compact cortical bone. These values were found to increase with age and, in older mice, were comparable to values previously reported for cortical bone BMD in mice (Windahl et al., 1999; Entezari et al., 2012). As we are reporting maximum BMD values, it is important to note that these are often higher than values reported in other studies quantifying mean BMD in ROIs that include both compact bone and marrow spaces.

In the present study, we provide several measures to evaluate the internal and external validity of our protocol. First, we measured the lengths of the tibia and femur to compare them with published values. Although seemingly straightforward, considerably different measurement methods have been previously reported. Many early studies measured mouse bone lengths using calipers or micrometer screw gauges (Somerville et al., 2004); others have used conventional radiographs, pQCT (Beamer et al., 1996), micro-CT (Amblard et al., 2003) or a combination of manual and imaging techniques (Bagi et al., 2006). However, precisely defined anatomical beginning and end points for measurements are not always described. We selected identifiable anatomical landmarks to consistently measure the long bones. Our findings correlate well with data from previous reports. Somerville et al. showed similar changes in tibial length with age in male C57BL/6 mice (Somerville et al., 2004). Somerville's study showed an ~20% increase in tibia length between 1 and 3 months of age, followed by a ~2.8% increase between 3 and 12 months of age (Somerville et al., 2004). Our data revealed a ~24% increase in tibia length between 1 and 3 months of age and an ~3.4% increase between 3 and 12 months of age. Femur lengths of our male mice showed similar patterns to that of other work in male C57BL/6 mice, with only small increases in bone length after 2 months of age (Glatt et al., 2007). Specifically, Glatt and coworkers showed an ~33% increase in femur length between 1 and 3 months of age, followed by a ~3.9% increase between 3 and 12 months (Glatt et al., 2007). Our data revealed ~30% increase in femur length between 1 and 3 months of age, followed by a ~6.5% increase between 3 and 12 months. These findings help validate our methodology and establish its reproducibility.

As a measure of internal validity, we compared CT-derived total body masses to gravimetrically measured masses at each age. These values were in good agreement, with the CT protocol underestimating total body weight by <3%. This finding helps establish the accuracy of our imaging and analysis methods for determining tissue masses.

To assess reproducibility, we scanned two separate cohorts of mice, both at 8 weeks of age, at different times using the same scanner and scanning protocol. These data revealed that the two cohorts of mice had nearly identical distributions of tissue and total body weights. Stability and reproducibility of the eXplore Locus Ultra micro-CT system itself has been previously shown (Du et al., 2007), further solidifying this assessment. In addition, we scanned one cohort of mice at 2, 5 and 8 weeks of age using two micro-CT systems. We found good agreement between WBC outputs from scanning on both systems, although it is evident that machine-specific performance parameters (*e.g.*, resolution and noise) can influence measurements. Taken together, our findings establish the validity and reproducibility of this approach for quantifying whole-body composition in studies of growth and aging in mice.

Our protocol offers a number of advantages. First, mice are anesthetized by isoflurane inhalation, which is less invasive with reduced adverse effects compared to anesthetic agents that are injected intraperitoneally (Szczesny et al., 2004; Fish et al., 2011). Mice recover quickly and repeated use of isoflurane is possible without noticeable harm. Scout scans can be used to determine precise positioning of animals prior to full scanning. Scans are non-invasive, rapid (as short as 16 s) and have low-radiation exposures. To establish the radiation safety of micro-CT scanning, a recent study demonstrated no significant effect on cardiac and pulmonary tissues in mice that were purposely delivered multiple exposures at triple the typical dose of radiation over a 6-week period (Detombe et al., 2013). Thus, repeated scans can be used to monitor changes over time in longitudinal studies with minimal concern for adverse effects of radiation. Moreover, analysis using this whole-body composition method is high-throughput.

There are also some limitations of our protocol that should be noted. To allow for accurate measurement of WBC and maintain an acceptably low radiation dose, the volumes required spatial averaging to lower resolutions (100 and 150 μm) to diminish noise levels in the images. Thus, in younger mice with smaller skeletons, skeletal mass and BMD may be underestimated due to under-mineralization and partial volume effects arising from increased isotropic voxel spacing. In addition, to quantify microarchitecture within the trabecular network of mouse bones, higher scan resolutions are required, as trabeculae are approximately 30–50 μm in width (Bouxsein et al., 2010). Thus, our *in vivo* scans at 50 μm are not capable of imaging small trabecular struts in mouse bones. Therefore, assessments of mouse bone microarchitecture must be performed at a scan resolution of ≤20 μm as post-mortem specimen scans.

Another limitation is that the earliest age that can be assessed is 2 weeks. It is not possible to obtain *in vivo* data from animals younger than this, as their bones are not sufficiently mineralized to perform quantifiable analyses at these resolutions. In contrast, micro-CT measurements of *ex vivo* murine fetal skeletons correlate well with standard histological techniques in mice as young as gestational day 17–19 (Oest et al., 2008). Furthermore, assessments of whole-mouse skeletons as young as 2 days of age are feasible when scanning post-mortem and with higher scan resolutions (Guldberg et al., 2004). To the best of our knowledge, *in vivo* micro-CT scanning prior to 2 weeks of age in mice has yet to be reported. It should also be noted that our studies were performed on mice with mixed genetic background and it is likely that our data would not exactly represent parameters in the original mouse strains. Consequently, it will be of interest in future studies to compare age-dependent changes in WBC of different strains of mice.

In summary, the present study is the first characterization of changes in WBC during growth and aging of mice using micro-CT. Our

findings provide critical reference data for other investigators using mice as disease models. Additionally, we show marked differences in WBC values during a period of rapid growth between 2 and 5 weeks of age, highlighting the importance of collecting data at precise ages when comparing groups within this range. Moreover, our study presents an in-depth analysis of WBC using an in-house-designed micro-CT protocol. This innovative methodology facilitates precise, long-term, repeated assessment of adipose, lean and skeletal tissues *in vivo* in growing and aging mice. Furthermore, our non-invasive method minimizes the use of research animals, as the mice can be scanned repeatedly. In addition, the 3D volumes enabled us to precisely measure growing long bones using consistent anatomical markers. Our findings establish that non-invasive single-energy micro-CT is an accurate and effective tool for high-throughput high-content characterization of WBC in mouse models.

Grants

This work was funded by the Canadian Institutes of Health Research (CIHR) [grant numbers 126065, 132377 and 133575]. K.L.B. was a supported by a Canadian Arthritis Network/The Arthritis Society Graduate Studentship and by the Joint Motion Program, a CIHR Strategic Training Program in Musculoskeletal Health Research and Leadership. D.W.H. holds the Dr. Sandy Kirkley Chair in Musculoskeletal Research at Western University.

Disclosures

No conflicts of interest, financial or otherwise, are declared by the authors.

Author contributions

Author contributions: K.L.B., S.J.D. and D.W.H. conceived and designed the research; K.L.B. performed the experiments; K.L.B. and S.I.P. analyzed the data; K.L.B., S.I.P., S.M.S., S.J.D. and D.W.H. interpreted results of the experiments; K.L.B. prepared the figures and drafted the manuscript; K.L.B., S.I.P., S.M.S., S.J.D. and D.W.H. edited and revised the manuscript, and approved the final version of the manuscript.

Acknowledgements

We thank Dr. Joseph Umoh for assistance with the scanning of mice, Vasek Pitelka for mouse anesthesia, Hristo Nikolov for providing the scanning cradles, Chris Norley for dosimetry and helpful advice on image analyses, and Oies Hussein for comments on the manuscript.

References

Amblard, D., Lafage-Proust, M.H., Laib, A., Thomas, T., Ruegsegger, P., Alexandre, C., Vico, L., 2003. Tail suspension induces bone loss in skeletally mature mice in the C57BL/6J strain but not in the C3H/HeJ strain. J. Bone Miner. Res. 18, 561–569. http://dx.doi.org/10.1359/jbmr.2003.18.3.561.

Bagi, C.M., Hanson, N., Andresen, C., Pero, R., Lariviere, R., Turner, C.H., Laib, A., 2006. The use of micro-CT to evaluate cortical bone geometry and strength in nude rats: correlation with mechanical testing, pQCT and DXA. Bone 38, 136–144. http://dx.doi.org/10.1016/j.bone.2005.07.028.

Beamer, W.G., Donahue, L.R., Rosen, C.J., Baylink, D.J., 1996. Genetic variability in adult bone density among inbred strains of mice. Bone 18, 397–403 (8756328296000476 [pii]).

Beaucage, K.L., Xiao, A., Pollmann, S.I., Grol, M.W., Beach, R.J., Holdsworth, D.W., Sims, S.M., Darling, M.R., Dixon, S.J., 2014. Loss of P2X7 nucleotide receptor function leads to abnormal fat distribution in mice. Purinergic Signal 10, 291–304. http://dx.doi.org/10.1007/s11302-013-9388-x.

Beck, J.A., Lloyd, S., Hafezparast, M., Lennon-Pierce, M., Eppig, J.T., Festing, M.F., Fisher, E.M., 2000. Genealogies of mouse inbred strains. Nat. Genet. 24, 23–25. http://dx.doi.org/10.1038/71641.

Bonkowski, M.S., Pamenter, R.W., Rocha, J.S., Masternak, M.M., Panici, J.A., Bartke, A., 2006. Long-lived growth hormone receptor knockout mice show a delay in age-related changes of body composition and bone characteristics. J. Gerontol. A Biol. Sci. Med. Sci. 61, 562–567 (61/6/562 [pii]).

Bouxsein, M.L., Boyd, S.K., Christiansen, B.A., Guldberg, R.E., Jepsen, K.J., Muller, R., 2010. Guidelines for assessment of bone microstructure in rodents using micro-computed tomography. J. Bone Miner. Res. 25, 1468–1486. http://dx.doi.org/10.1002/jbmr.141.

Brochmann, E.J., Duarte, M.E., Zaidi, H.A., Murray, S.S., 2003. Effects of dietary restriction on total body, femoral, and vertebral bone in SENCAR, C57BL/6, and DBA/2 mice. Metabolism 52, 1265–1273 (S002604950300194X [pii]).

Brodt, M.D., Ellis, C.B., Silva, M.J., 1999. Growing C57Bl/6 mice increase whole bone mechanical properties by increasing geometric and material properties. J. Bone Miner. Res. 14, 2159–2166. http://dx.doi.org/10.1359/jbmr.1999.14.12.2159.

Buie, H.R., Campbell, G.M., Klinck, R.J., MacNeil, J.A., Boyd, S.K., 2007. Automatic segmentation of cortical and trabecular compartments based on a dual threshold technique for in vivo micro-CT bone analysis. Bone 41, 505–515. http://dx.doi.org/10.1016/j.bone.2007.07.007.

Buie, H.R., Moore, C.P., Boyd, S.K., 2008. Postpubertal architectural developmental patterns differ between the L3 vertebra and proximal tibia in three inbred strains of mice. J. Bone Miner. Res. 23, 2048–2059. http://dx.doi.org/10.1359/jbmr.080808.

Cheung, A.M., Adachi, J.D., Hanley, D.A., Kendler, D.L., Davison, K.S., Josse, R., Brown, J.P., Ste-Marie, L.G., Kremer, R., Erlandson, M.C., Dian, L., Burghardt, A.J., Boyd, S.K., 2013. High-resolution peripheral quantitative computed tomography for the assessment of bone strength and structure: a review by the Canadian Bone Strength Working Group. Curr. Osteoporos. Rep. 11, 136–146. http://dx.doi.org/10.1007/s11914-013-0140-9.

Crawley, J.N., Belknap, J.K., Collins, A., Crabbe, J.C., Frankel, W., Henderson, N., Hitzemann, R.J., Maxson, S.C., Miner, L.L., Silva, A.J., Wehner, J.M., Wynshaw-Boris, A., Paylor, R., 1997. Behavioral phenotypes of inbred mouse strains: implications and recommendations for molecular studies. Psychopharmacology 132, 107–124.

Detombe, S.A., Dunmore-Buyze, J., Petrov, I.E., Drangova, M., 2013. X-ray dose delivered during a longitudinal micro-CT study has no adverse effect on cardiac and pulmonary tissue in C57BL/6 mice. Acta Radiol. 54, 435–441. http://dx.doi.org/10.1177/0284185113475608.

Donnelly, E., 2011. Methods for assessing bone quality: a review. Clin. Orthop. Relat. Res. 469, 2128–2138. http://dx.doi.org/10.1007/s11999-010-1702-0.

Dougherty, G., 1996. Quantitative CT in the measurement of bone quantity and bone quality for assessing osteoporosis. Med. Eng. Phys. 18, 557–568 (1350453396000112 [pii]).

Du, L.Y., Umoh, J., Nikolov, H.N., Pollmann, S.I., Lee, T.Y., Holdsworth, D.W., 2007. A quality assurance phantom for the performance evaluation of volumetric micro-CT systems. Phys. Med. Biol. 52, 7087–7108. http://dx.doi.org/10.1088/0031-9155/52/23/021.

Entezari, V., Vartanians, V., Zurakowski, D., Patel, N., Fajardo, R.J., Muller, R., Snyder, B.D., Nazarian, A., 2012. Further improvements on the factors affecting bone mineral density measured by quantitative micro-computed tomography. Bone 50, 611–618. http://dx.doi.org/10.1016/j.bone.2011.10.004.

Fish, R., Danneman, P.J., Brown, M., Karas, A., 2011. Anesthesia and Analgesia in Laboratory Animals. 2 ed. Academic Press, London, UK.

Ford-Hutchinson, A.F., Cooper, D.M., Hallgrimsson, B., Jirik, F.R., 2003. Imaging skeletal pathology in mutant mice by microcomputed tomography. J. Rheumatol. 30, 2659–2665 (0315162X-30-2659 [pii]).

Glatt, V., Canalis, E., Stadmeyer, L., Bouxsein, M.L., 2007. Age-related changes in trabecular architecture differ in female and male C57BL/6J mice. J. Bone Miner. Res. 22, 1197–1207. http://dx.doi.org/10.1359/jbmr.070507.

Granton, P.V., Norley, C.J., Umoh, J., Turley, E.A., Frier, B.C., Noble, E.G., Holdsworth, D.W., 2010. Rapid in vivo whole body composition of rats using cone beam μCT. J. Appl. Physiol. 109, 1162–1169. http://dx.doi.org/10.1152/japplphysiol.00016.2010.

Guldberg, R.E., Lin, A.S., Coleman, R., Robertson, G., Duvall, C., 2004. Microcomputed tomography imaging of skeletal development and growth. Birth Defects Res. C Embryo Today 72, 250–259. http://dx.doi.org/10.1002/bdrc.20016.

Halldorsdottir, S., Carmody, J., Boozer, C.N., Leduc, C.A., Leibel, R.L., 2009. Reproducibility and accuracy of body composition assessments in mice by dual energy x-ray absorptiometry and time domain nuclear magnetic resonance. Int. J. Body Compos. Res. 7, 147–154.

Halloran, B.P., Ferguson, V.L., Simske, S.J., Burghardt, A., Venton, L.L., Majumdar, S., 2002. Changes in bone structure and mass with advancing age in the male C57BL/6J mouse. J. Bone Miner. Res. 17, 1044–1050. http://dx.doi.org/10.1359/jbmr.2002.17.6.1044.

Hankenson, F.C., Garzel, L.M., Fischer, D.D., Nolan, B., Hankenson, K.D., 2008. Evaluation of tail biopsy collection in laboratory mice (*Mus musculus*): vertebral ossification, DNA quantity, and acute behavioral responses. J. Am. Assoc. Lab. Anim. Sci. 47, 10–18.

ICRU, 1989. Tissue substitutes in radiation dosimetry and measurements. ICRU Report 44. International Commission on Radiation Units and Measurements, Bethesda, MD.

Ito, M., 2005. Assessment of bone quality using micro-computed tomography (micro-CT) and synchrotron micro-CT. J. Bone Miner. Metab. 23, 115–121 (Suppl).

Ito, M., Ejiri, S., Jinnai, H., Kono, J., Ikeda, S., Nishida, A., Uesugi, K., Yagi, N., Tanaka, M., Hayashi, K., 2003. Bone structure and mineralization demonstrated using synchrotron radiation computed tomography (SR-CT) in animal models: preliminary findings. J. Bone Miner. Metab. 21, 287–293. http://dx.doi.org/10.1007/s00774-003-0422-x.

Judex, S., Boyd, S., Qin, Y.X., Miller, L., Muller, R., Rubin, C., 2003. Combining high-resolution micro-computed tomography with material composition to define the quality of bone tissue. Curr. Osteoporos. Rep. 1, 11–19.

Kazakia, G.J., Burghardt, A.J., Cheung, S., Majumdar, S., 2008. Assessment of bone tissue mineralization by conventional x-ray microcomputed tomography: comparison with synchrotron radiation microcomputed tomography and ash measurements. Med. Phys. 35, 3170–3179.

Kohn, H.I., Kallman, R.F., 1957. The influence of strain on acute x-ray lethality in the mouse. II. Recovery rate studies. Radiat. Res. 6, 329–338.

Kozak, L.P., Koza, R.A., Anunciado-Koza, R., 2010. Brown fat thermogenesis and body weight regulation in mice: relevance to humans. Int. J. Obes. 34 (Suppl. 1), S23–S27. http://dx.doi.org/10.1038/ijo.2010.179.

MacNeil, J.A., Boyd, S.K., 2007. Accuracy of high-resolution peripheral quantitative computed tomography for measurement of bone quality. Med. Eng. Phys. 29, 1096–1105. http://dx.doi.org/10.1016/j.medengphy.2006.11.002.

Martin-Badosa, E., Amblard, D., Nuzzo, S., Elmoutaouakkil, A., Vico, L., Peyrin, F., 2003. Excised bone structures in mice: imaging at three-dimensional synchrotron radiation micro CT. Radiology 229, 921–928. http://dx.doi.org/10.1148/radiol.2293020558.

Migliaccio, S., Greco, E.A., Wannenes, F., Donini, L.M., Lenzi, A., 2014. Adipose, bone and muscle tissues as new endocrine organs: role of reciprocal regulation for osteoporosis and obesity development. Horm. Mol. Biol. Clin. Investig. 17, 39–51. http://dx.doi.org/10.1515/hmbci-2013-0070.

Miller, L.M., Little, W., Schirmer, A., Sheik, F., Busa, B., Judex, S., 2007. Accretion of bone quantity and quality in the developing mouse skeleton. J. Bone Miner. Res. 22, 1037–1045. http://dx.doi.org/10.1359/jbmr.070402.

Mole, R.H., 1957. Quantitative observations on recovery from whole body irradiation in mice. II. Recovery during and after daily irradiation. Br. J. Radiol. 30, 40–46. http://dx.doi.org/10.1259/0007-1285-30-349-40.

Oest, M.E., Jones, J.C., Hatfield, C., Prater, M.R., 2008. Micro-CT evaluation of murine fetal skeletal development yields greater morphometric precision over traditional clear-staining methods. Birth Defects Res. B Dev. Reprod. Toxicol. 83, 582–589. http://dx.doi.org/10.1002/bdrb.20177.

Parkins, C.S., Fowler, J.F., Maughan, R.L., Roper, M.J., 1985. Repair in mouse lung for up to 20 fractions of X rays or neutrons. Br. J. Radiol. 58, 225–241. http://dx.doi.org/10.1259/0007-1285-58-687-225.

Pietrobelli, A., Formica, C., Wang, Z., Heymsfield, S.B., 1996. Dual-energy X-ray absorptiometry body composition model: review of physical concepts. Am. J. Phys. 271, E941–E951.

Pisani, P., Renna, M.D., Conversano, F., Casciaro, E., Muratore, M., Quarta, E., Paola, M.D., Casciaro, S., 2013. Screening and early diagnosis of osteoporosis through X-ray and ultrasound based techniques. World J. Radiol. 5, 398–410. http://dx.doi.org/10.4329/wjr.v5.i11.398.

Raum, K., Hofmann, T., Leguerney, I., Saied, A., Peyrin, F., Vico, L., Laugier, P., 2007. Variations of microstructure, mineral density and tissue elasticity in B6/C3H mice. Bone 41, 1017–1024. http://dx.doi.org/10.1016/j.bone.2007.08.042.

Richman, C., Kutilek, S., Miyakoshi, N., Srivastava, A.K., Beamer, W.G., Donahue, L.R., Rosen, C.J., Wergedal, J.E., Baylink, D.J., Mohan, S., 2001. Postnatal and pubertal skeletal changes contribute predominantly to the differences in peak bone density between C3H/HeJ and C57BL/6J mice. J. Bone Miner. Res. 16, 386–397. http://dx.doi.org/10.1359/jbmr.2001.16.2.386.

Rosenthal, N., Brown, S., 2007. The mouse ascending: perspectives for human-disease models. Nat. Cell Biol. 9, 993–999. http://dx.doi.org/10.1038/ncb437.

Sato, F., Sasaki, S., Kawashima, N., Chino, F., 1981. Late effects of whole or partial body x-irradiation on mice: life shortening. Int. J. Radiat. Biol. Relat. Stud. Phys. Chem. Med. 39, 607–615.

Senn, S.M., Kantor, S., Leury, B.J., Andrikopoulos, S., O'Brien, T.J., Morris, M.J., Proietto, J., Wark, J.D., 2007. In vivo quantification of fat content in mice using the Hologic QDR 4500A densitometer. Obes. Res. Clin. Pract. 1, 1–78. http://dx.doi.org/10.1016/j.orcp.2006.11.001.

Sheng, M.H., Baylink, D.J., Beamer, W.G., Donahue, L.R., Rosen, C.J., Lau, K.H., Wergedal, J.E., 1999. Histomorphometric studies show that bone formation and bone mineral apposition rates are greater in C3H/HeJ (high-density) than C57BL/6J (low-density) mice during growth. Bone 25, 421–429 (S8756-3282(99)00184-2 [pii]).

Sjogren, K., Hellberg, N., Bohlooly, Y.M., Savendahl, L., Johansson, M.S., Berglindh, T., Bosaeus, I., Ohlsson, C., 2001. Body fat content can be predicted in vivo in mice using a modified dual-energy X-ray absorptiometry technique. J. Nutr. 131, 2963–2966.

Somerville, J.M., Aspden, R.M., Armour, K.E., Armour, K.J., Reid, D.M., 2004. Growth of C57BL/6 mice and the material and mechanical properties of cortical bone from the tibia. Calcif. Tissue Int. 74, 469–475. http://dx.doi.org/10.1007/s00223-003-0101-x.

Szczesny, G., Veihelmann, A., Massberg, S., Nolte, D., Messmer, K., 2004. Long-term anaesthesia using inhalatory isoflurane in different strains of mice-the haemodynamic effects. Lab. Anim. 38, 64–69. http://dx.doi.org/10.1258/00236770460734416.

Tagliaferri, C., Wittrant, Y., Davicco, M.J., Walrand, S., Coxam, V., 2015. Muscle and bone, two interconnected tissues. Ageing Res. Rev. 21, 55–70. http://dx.doi.org/10.1016/j.arr.2015.03.002.

White, D.R., 1978. Tissue substitutes in experimental radiation physics. Med. Phys. 5, 467–479.

Windahl, S.H., Vidal, O., Andersson, G., Gustafsson, J.A., Ohlsson, C., 1999. Increased cortical bone mineral content but unchanged trabecular bone mineral density in female $ER\beta^{-/-}$ mice. J. Clin. Invest. 104, 895–901. http://dx.doi.org/10.1172/JCI6730.

Wyatt, S.K., Barck, K.H., Kates, L., Zavala-Solorio, J., Ross, J., Kolumam, G., Sonoda, J., Carano, R.A., 2015. Fully-automated, high-throughput micro-computed tomography analysis of body composition enables therapeutic efficacy monitoring in preclinical models. Int. J. Obes. 39, 1630–1637. http://dx.doi.org/10.1038/ijo.2015.113.

Xue, B., Rim, J.S., Hogan, J.C., Coulter, A.A., Koza, R.A., Kozak, L.P., 2007. Genetic variability affects the development of brown adipocytes in white fat but not in interscapular brown fat. J. Lipid Res. 48, 41–51. http://dx.doi.org/10.1194/jlr.M600287-JLR200.